The 9th European Congress on Computational Methods in Applied Sciences and Engineering
ECCOMAS Congress 2024
3–7 June 2024, Lisboa, Portugal

THINNING-INDUCED BREAKUP OF A GRAVITATIONAL LIQUID JET DRIVEN BY VARICOSE PERTURBATIONS

Alessandro Della Pia[1], Matteo Chiatto[2] and Luigi de Luca [2]

[1] Scuola Superiore Meridionale, School for Advanced Studies,
Naples, 80128, Italy
email: alessandro.dellapia@unina.it

[2] University of Naples "Federico II", Department of Industrial Engineering,
Naples, 80125, Italy
email: matteo.chiatto@unina.it, deluca@unina.it

Key words: volume-of-fluid, scaling laws, two-phase flow

Summary. We study numerically the varicose dynamics of a forced gravitational liquid sheet (curtain) issuing into a quiescent gaseous ambient. The investigation is performed in supercritical regime, namely for Weber number $We > 1$. Two methodologies are employed: a simplified one-dimensional (1D) linear model and two-dimensional (2D) volume-of-fluid simulations. Using harmonic forcing perturbations of the streamwise velocity applied at the inlet section, the curtain varicose dynamics is excited by varying the forcing frequency f and amplitude A_u of the perturbations for different values of We. The 1D analysis reveals that the curtain oscillations amplitude reaches a maximum value for a certain forcing frequency $f = f_{max}$. In other terms, it is found that the flow manifests a resonance behaviour, with the natural oscillation frequency f_{max} and corresponding amplitude $A_{h,max}$ both scaling as $We^{\frac{1}{3}}$, while the average wavelength $\bar{\lambda}_{max}$ scales as $We^{-\frac{1}{3}}$. It is found that the 2D curtain breaks up numerically by increasing the forcing amplitude A_u in resonance conditions. The numerical rupture is determined by a progressive curtain thinning induced by the varicose deformation, which moves upstream by increasing We, i.e. downstream by increasing the surface tension coefficient. In this respect, surface tension is found to play a stabilizing role on the varicose oscillations of the curtain.

1 Introduction

The stability and dynamics of gravitational liquid sheets (curtains) interacting with an initially quiescent gaseous ambient have been investigated by the scientific community for decades ([1]). Within a linear mathematical framework, [2] showed two linearly independent wave modes of a liquid sheet, namely sinuous and varicose modes, which were then experimentally observed by [3]. The sinuous mode moves the two free surfaces of the curtain in phase, while the varicose one symmetrically moves the free surfaces in opposite directions (see Fig. 1).

The development of two-phase flow direct numerical simulations and modal decomposition techniques has recently allowed to disclose new aspects of liquid sheets unsteady dynamics, both in supercritical ($We > 1$) and subcritical ($We < 1$) regimes. A linear destabilization mechanism of sinuous modes based on the interaction between the liquid phase and the surrounding gaseous environment has been detected in supercritical conditions by [4], who derived the eigenvalues

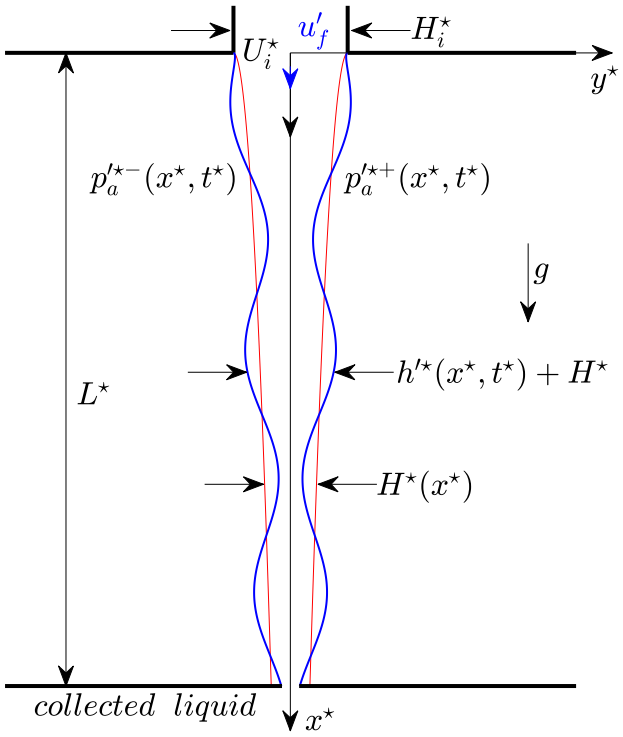

Figure 1: Sketch of the gravitational liquid sheet (curtain) flow. The forcing term u'_f superposed to the base flow (red lines) excites the varicose deformation of the curtain shape (blue lines).

spectrum of the one-dimensional curtain flow and showed it is unstable when the density ratio r_ρ exceeds a threshold value. This result was confirmed by [5], who derived the BiGlobal spectrum of the curtain flow by performing a dynamic mode decomposition analysis based on two-dimensional nonlinear simulation data. For $We < 1$, an energy budget decomposition analysis of the curtain flow recently performed by [6] identified surface tension as a possible physical mechanism responsible for the sinuous modes instability in subcritical conditions, as the Weber number is progressively decreased down to We_{th}. The threshold Weber number We_{th} was defined as the We value for which the sheet is entirely subcritical (local Weber number less than unity everywhere along the curtain). In these conditions, a transient algebraic growth of perturbations was found in both asymptotically stable ($We_{th} < We < 1$) and unstable ($We < We_{th}$) regimes, thus retrieving previous results by [7] and [8].

From the literature review summarized above, it arises that the sinuous dynamics of gravitational liquid sheets has been deeply investigated over the years by means of theoretical, numerical and experimental approaches, both for $We > 1$ and $We < 1$. On the contrary, a corresponding systematic characterization of the varicose dynamics of this class of flows still needs to be improved in the literature. The topic is particularly relevant for industrial processes such as coating deposition ([9]). In this application, it is fundamental to maintain the curtain stable during the whole process. Varicose perturbations of the curtain interfaces can arise due to fluctuations of the streamwise velocity component coming from the liquid pump, which is placed upstream of the coating die used to deliver the fluid and to form the curtain.

This work aims to provide a numerical characterization of the varicose dynamics of a gravi-

tational liquid sheet, which is excited by harmonic disturbances of the inlet streamwise velocity component u. The investigation is performed in a supercritical regime ($We > 1$) through a simplified one-dimensional linear model (Section 2.1) and two-dimensional volume-of-fluid simulations (Section 2.2). The first results are shown in Section 3, where the varicose dynamics is explored by varying the forcing frequency f and the Weber number We, thus identifying different flow conditions depending on the specific values of the two parameters. Afterwards, the effect of the forcing amplitude A_u is investigated in Section 4, focusing attention on the most relevant flow conditions outlined in the first part of the analysis. Conclusions are finally drawn in Section 5.

2 Physical layout and methodologies

The gravitational liquid sheet (curtain) flow here considered is schematically reported in Fig. 1. In the unperturbed configuration, the curtain issues vertically (along the $x^\star$ direction) into a quiescent gaseous ambient, and it is characterized by a steady velocity distribution and two symmetrical free interfaces (red lines in Fig. 1). Due to the gravitational acceleration g, the unperturbed thickness distribution $H^\star$ decreases by moving downstream along $x^\star$. A streamwise velocity perturbation u'_f is introduced at the inlet section ($x^\star = 0$) and excites the sheet unsteady dynamics, which is characterized by a varicose (i.e. symmetric with respect to $x^\star$) displacement of the right ($y^{\star+}$) and left ($y^{\star-}$) interfaces (blue lines in Fig. 1). The total thickness distribution $h^\star(x^\star, t^\star)$ thus results in the sum of the base flow $H^\star(x^\star)$ and the induced perturbation $h'^\star(x^\star, t^\star)$. In terms of the curtain interfaces positions, it is given as

$$h^\star(x^\star, t^\star) = y^{\star+}(x^\star, t^\star) - y^{\star-}(x^\star, t^\star). \tag{1}$$

2.1 One-dimensional linear modelling

Starting from the two-dimensional Euler equations closed by kinematic and dynamic conditions imposed at the free interfaces, a simplified inviscid model of the varicose curtain dynamics is hereafter derived.

The simplifying assumptions are the same as those made by [4] to study the sinuous dynamics of this class of flows. The unperturbed curtain configuration is assumed to be thin with respect to the wavelength of superposed disturbances, so that velocity profiles can be considered locally uniform across the sheet thickness (one-dimensional flow assumption). The generic unsteady quantity, $\phi^\star$, is considered as the sum of a steady contribution and a perturbation, $\phi^\star = \Phi^\star + \phi'^\star$. Note that the apex $\star$ denotes, here as elsewhere, dimensional quantities. Within the approximation of small perturbations, the mass and $x^\star$-momentum balances are formulated by neglecting the products of perturbations terms (linear flow assumption) and then integrated along $y^\star$, and read as

$$\frac{\partial h'^\star}{\partial t^\star} = -\frac{\partial}{\partial x^\star}\left(U^\star h'^\star + H^\star u'^\star\right), \tag{2}$$

$$\frac{\partial u'^\star}{\partial t^\star} + \frac{\partial}{\partial x^\star}\left(U^\star u'^\star\right) = \frac{\sigma}{2\rho_l}\frac{\partial^3 h'^\star}{\partial x^{\star 3}} - \frac{1}{2\rho_l}\frac{\partial(p_a'^{\star+} + p_a'^{\star-})}{\partial x^\star}, \tag{3}$$

being

$$p_a'^{\star+} + p_a'^{\star-} = -\frac{\rho_a}{\pi} \int_0^{L^\star} \frac{\partial^2 h'^\star}{\partial t^{\star 2}} \ln \left| \frac{x^\star - \xi^\star}{L^\star} \right| d\xi^\star. \tag{4}$$

In Eqs. (2)-(3), $H^\star$ and $U^\star$ are the base flow thickness and velocity distributions, respectively, while $h'^\star$ and $u'^\star$ the corresponding perturbations. Moreover, $L^\star$ is the curtain length, ρ_l, ρ_a and σ stand for the liquid density, the gaseous ambient density, and the surface tension coefficient, respectively, and $t^\star$ denotes the time. Note that the symbol $\xi^\star$ in Eq. (4) denotes the spatial integration variable, which spans the entire liquid sheet length $L^\star$. The curtain and gaseous ambient dynamics are thus coupled through the integral term represented by Eq. (4), being the local ambient pressure perturbations dependent on the global liquid sheet deformation.

The dimensionless form of Eqs. (2)-(3) is finally obtained,

$$\frac{\partial h'}{\partial t} + U\frac{\partial h'}{\partial x} = -\frac{\varepsilon}{U}\frac{\partial u'}{\partial x} - h'\frac{\partial U}{\partial x} + \frac{\varepsilon u'}{U^2}\frac{\partial U}{\partial x}, \tag{5}$$

$$\frac{\partial u'}{\partial t} + U\frac{\partial u'}{\partial x} = -u'\frac{\partial U}{\partial x} + \frac{\varepsilon}{4We}\frac{\partial^3 h'}{\partial x^3} + \frac{r_\rho}{2\pi}\frac{\partial}{\partial x}\int_0^1 \frac{\partial^2 h'}{\partial t^2} \ln|x-\xi|\, d\xi, \tag{6}$$

where Eq. (4) has been replaced into Eq. (3), and the following dimensionless parameters,

$$We = \frac{\rho_l U_i^{\star 2} H_i^\star}{2\sigma}, \quad Fr = \frac{U_i^{\star 2}}{gL^\star}, \quad \varepsilon = \frac{H_i^\star}{L^\star}, \quad r_\rho = \frac{\rho_a}{\rho_l}, \tag{7}$$

and non-dimensional variables,

$$H = \frac{H^\star}{H_i^\star}, \quad U = \frac{U^\star}{U_i^\star}, \quad h' = \frac{h'^\star}{H_i^\star}, \quad u' = \frac{u'^\star}{\varepsilon U_i^\star}, \quad x = \frac{x^\star}{L^\star}, \quad t = \frac{t^\star U_i^\star}{L^\star}, \tag{8}$$

have been introduced. In Eq. (7), We is the Weber number, Fr the Froude number, ε the curtain slenderness ratio and r_ρ the density ratio. Based on the works by [10] and [11], the Torricelli's free-fall model,

$$U = \sqrt{1 + \frac{2}{Fr}x}, \tag{9}$$

is employed as the base flow in Eqs. (5)-(6).

The two unknowns in Eqs. (5)-(6) are the spatio-temporal evolutions of the curtain thickness ($h'(x,t)$) and velocity ($u'(x,t)$) perturbations. The system (5)-(6) is thus closed by assigning the following inlet boundary conditions,

$$h'(0,t) = 0, \tag{10}$$

$$u'(0,t) = u'_f = \frac{A_u}{\varepsilon}\sin(2\pi f t), \tag{11}$$

the free-outflow condition at the outlet section ($x = 1$) being self-guaranteed. The coefficients $A_u = A_u^\star/U_i^\star$ and $f = f^\star L^\star/U_i^\star$ in Eq. (11) represent the amplitude and frequency of the harmonic forcing, respectively. As it will be shown in Section 3, adding the forcing perturbation (Eq. (11)) allows one to identify the natural frequencies of the varicose dynamics by searching for the resonance conditions of the curtain flow.

The numerical resolution of the system (5)-(6) equipped with boundary conditions (10)-(11) is performed by means of a standard finite-difference discretization method in MATLAB. Note that, for any $x = \xi$, the integrand in Eq. (6) is singular, and its evaluation requires a suitable treatment ([12]).

2.2 Two-dimensional volume-of-fluid simulations

The two-dimensional two-phase flow field represented by the liquid curtain interacting with the initially quiescent gaseous environment is modelled through the one-fluid formulation of incompressible Navier-Stokes equations ([13]), reading as

$$\frac{\partial u_i^\star}{\partial x_i^\star} = 0, \tag{12a}$$

$$\rho\left(\frac{\partial u_i^\star}{\partial t^\star} + u_j^\star \frac{\partial u_i^\star}{\partial x_j^\star}\right) = -\frac{\partial p^\star}{\partial x_i^\star} + \rho g_i + \frac{\partial}{\partial x_j^\star}\left[\mu\left(\frac{\partial u_i^\star}{\partial x_j^\star} + \frac{\partial u_j^\star}{\partial x_i^\star}\right)\right] + \sigma\kappa^\star n_i \delta_S, \tag{12b}$$

$$\frac{\partial C}{\partial t^\star} + \frac{\partial C u_i^\star}{\partial x_i^\star} = 0. \tag{12c}$$

The vectors $\mathbf{u}^\star = (u^\star, v^\star)$ and $\mathbf{g} = (g, 0)$ represent the flow velocity and the gravitational acceleration, respectively, $p^\star$ the pressure field, $\kappa^\star$ the mean gas-liquid interface curvature, and $\mathbf{n} = (n_x, n_y)$ the outward pointing normal vector to the interface. The Dirac distribution function δ_S is equal to 1 at the interface, and 0 elsewhere. The density ρ and viscosity μ fields are discontinuous across the interface separating the two fluids,

$$\rho = \rho_a + (\rho_l - \rho_a)C, \tag{13a}$$

$$\mu = \mu_a + (\mu_l - \mu_a)C, \tag{13b}$$

being the volume fraction C a discontinuous function, which is equal to either 1 or 0 in the liquid or gaseous regions, respectively.

Eqs. (12a)-(12c) are solved using BASILISK, an improved version of the open-source code Gerris ([14]) extensively used and validated for plane liquid jet flow problems ([15, 16], [17]). The code employs the volume-of-fluid (VOF) method by [13] to track the interface on a quadtree structured grid, with an adaptive mesh refinement based on a criterion of wavelet-estimated discretization error ([18]) and no special treatment required in presence of liquid phase breakup ([19]). A multigrid solver is employed to satisfy the incompressibility condition, while the calculation of the surface tension term is based on the balanced continuum surface force technique ([20]), which is coupled with a height-function curvature estimation method to avoid the generation of spurious currents. For exhaustive details about the code BASILISK, the reader is referred to [14, 21] and to the software official website (`http://basilisk.fr`).

The computational domain employed to calculate two-dimensional curtain flow solutions is a square, whose length side is equal to the curtain length $L^\star$. The liquid sheet shape is initialized as a rectangle of area $L^\star \times H_i^\star$ at $t = 0$. Inflow boundary conditions are prescribed at the inlet: at the curtain slot exit section ($-1/2 < y < 1/2$, where $y = y^\star/H_i^\star$), they read as

$$u = \begin{cases} \dfrac{3}{2}\left(1 - 4y^2\right), & t \le t_{steady}, \\ \dfrac{3}{2}\left(1 - 4y^2\right) + u_f'(t), & t > t_{steady}, \end{cases} \tag{14a}$$

$$v = 0, \tag{14b}$$

$$C = 1, \tag{14c}$$

while the values $u = v = C = 0$ are enforced for $|y| > 1/2$. Note that the streamwise velocity boundary condition, Eq. (14a), is the sum of a steady contribution, corresponding to a fully developed parabolic velocity profile, and an unsteady perturbation $u'_f(t)$. The latter term represents the harmonic forcing (previously defined by Eq. (11)) exciting the curtain varicose dynamics after the steady base flow solution is achieved, for which a computational time equal to $t_{steady} \approx 1.5$ is required. A standard free-outflow boundary condition is enforced at the outlet, namely $p = \partial u/\partial x = \partial v/\partial x = \partial C/\partial x = 0$, while homogeneous Neumann boundary conditions for all variables are enforced on the remaining sides of the domain.

A quadtree-structured grid is employed in the computations, which is characterized by a maximum level of refinement $LoR = 10$ in a rectangular region containing the entire liquid sheet, and by a dynamical refinement of the cells elsewhere in the domain according to user-defined adaptation criteria ([18]). In particular, the refinement of a generic grid cell is performed at each iteration reducing by one and then increasing again its grid level, resulting in a down- and up-sampling of the stored scalar fields. Therefore, the error $\chi = ||\phi - \phi^+||$ between the original (ϕ) and the up-sampled (ϕ^+) fields can be estimated; the cell is refined if $\chi > \beta$ and coarsened if $\chi < \beta$, where β is the error threshold of the specific scalar field. For all simulations reported herein, the value $\beta = 1.0 \times 10^{-4}$ has been prescribed for both the velocity components and the volume fraction field. The maximum LoR employed here gives a minimum cell size equal to $\Delta x^\star = 0.05 H_i^\star$, which corresponds to 20 grid cells within $H_i^\star$.

3 Frequency response of 1D varicose dynamics

The forcing frequency f effect on the one-dimensional curtain flow stationary (i.e. long-time) solution obtained for Weber number $We = 2.5$ and forcing velocity amplitude $A_u = 0.1$ is first considered; results are reported in Fig. 2. In particular, Fig. 2(a) shows the curtain perturbation thickness spatial distribution $h'(x)$ for three significant values of the forcing frequency, namely $f = 0.76$ (black curve), $f = 5.34$ (red curve) and $f = 11.43$ (blue curve), while the complete frequency response (i.e. the oscillations amplitude) is reported in Fig. 2(b) as a function of f, for a broad range of forcing frequency values ($f \in [0.15, 15]$). Note that the function $A_h(f)$ has been scaled with respect to its maximum value $A_{h,max} = 0.21$.

The non-parallelism of the base flow $U(x)$ due to the gravitational acceleration (see Eq. (9)) determines a spatial variation of the wavelength $\lambda = \lambda^\star/L^\star$ of the curtain thickness perturbation $h'(x)$, which increases by moving downstream along the curtain ($\lambda(x) = U(x)/f$), as shown in Fig. 2(a). By considering the average value of the base flow $\bar{U} = 1.96$ as a reference velocity, one can estimate the average wavelength $\bar{\lambda} = \bar{U}/f$ corresponding to each case. It is thus obtained that $\bar{\lambda} = 2.57$, 0.37 and 0.17 for $f = 0.76$, 5.34 and 11.43, respectively, which well represents the distance between two consecutive peaks of the $h'(x)$ distribution (see in particular red and blue curves in Fig. 2(a), for which $\bar{\lambda} < 1$). Moreover, the analysis of Fig. 2(b) reveals that the oscillation amplitude reaches a maximum value equal to $A_{h,max} = 0.21$ at the forcing frequency $f = 5.34$. Therefore, as a significant result of the present investigation, it is found that the value $f = 5.34$ represents the resonance (and thus the natural) frequency of the flow system for $We = 2.5$, being the trend $A_h(f)$ peaked at $f_{max} = 5.34$ (red dashed line in Fig. 2(b)).

The varicose oscillatory dynamics of the forced flow is further investigated in Fig. 3, where the Weber number effect on the whole frequency response $A_h(f)$ (panel (a)), the resonance frequency f_{max} (panel (b)) and the corresponding amplitude $A_{h,max}$ (panel (c)) are reported in

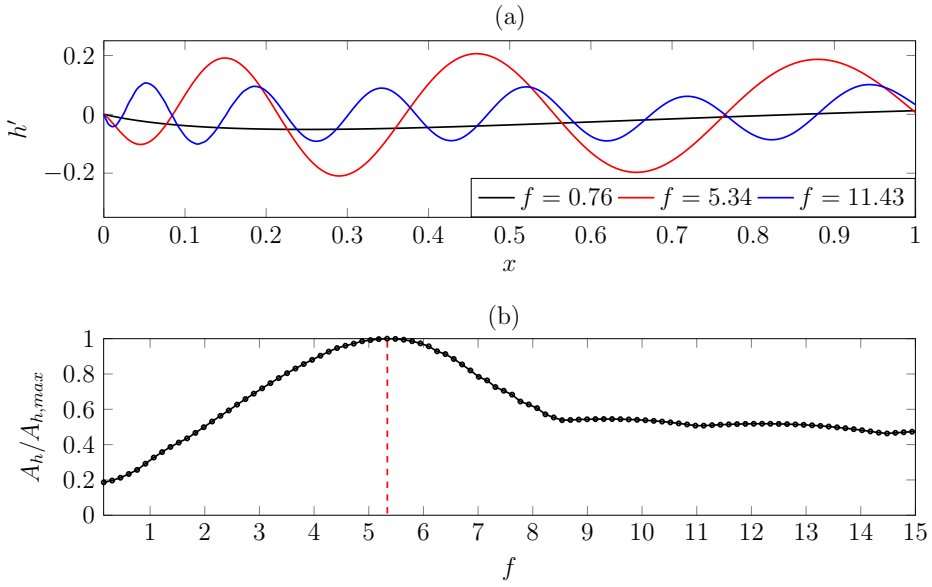

Figure 2: Forcing frequency f effect on the curtain perturbation thickness spatial distribution $h'(x)$ (panel(a)) and on its maximum temporal oscillations amplitude A_h scaled with respect to the value $A_{h,max} = 0.21$ (panel(b)). The red dashed line in panel (b) denotes the peak frequency $f_{max} = 5.34$. Here, $We = 2.5$ and $A_u = 0.1$.

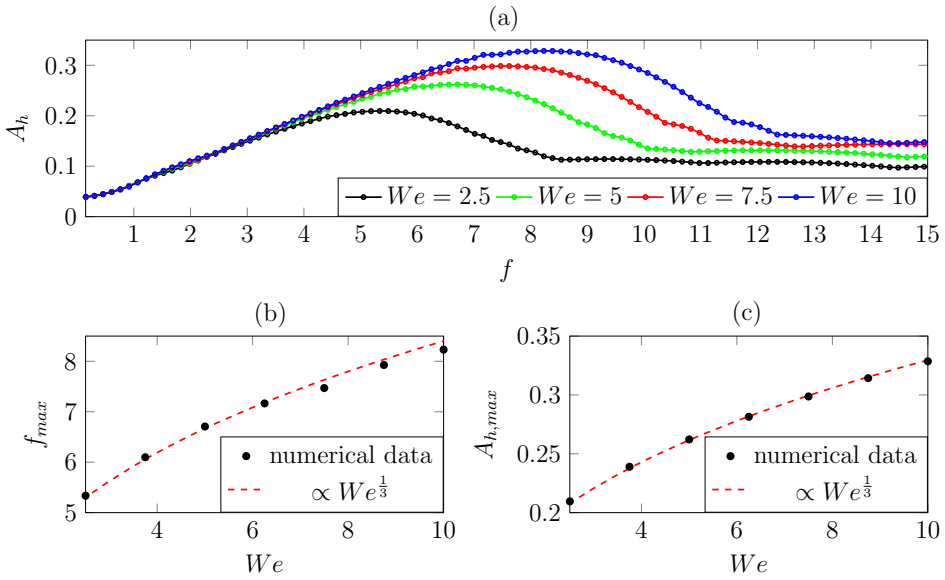

Figure 3: Frequency response in terms of curtain perturbation thickness A_h as a function of the forcing frequency f (panel(a)); peak frequency f_{max} (panel (b)) and corresponding amplitude $A_{h,max}$ (panel (c)) variations with the Weber number We. Here, the forcing amplitude is $A_u = 0.1$.

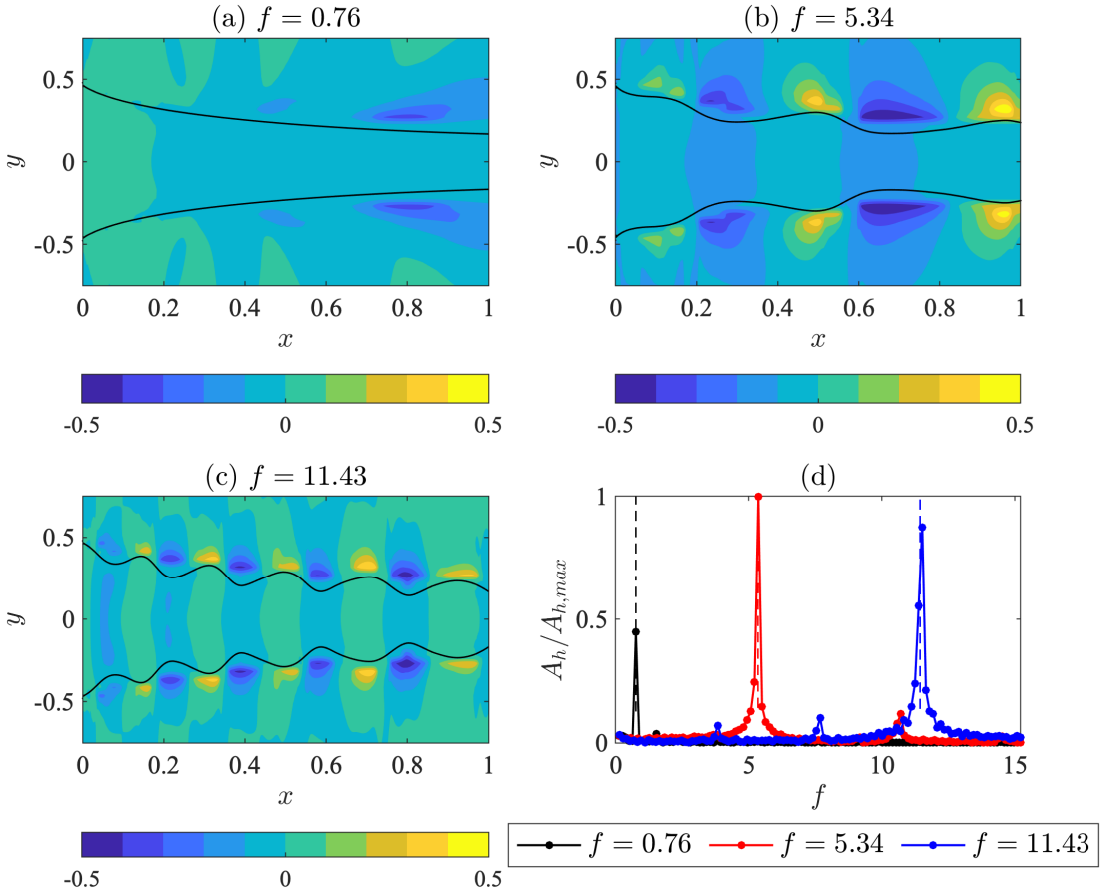

Figure 4: VOF simulations of two-dimensional curtain flow: streamwise velocity perturbation u' contour (panels (a)-(c)) and Fast Fourier Transform of the thickness perturbation h' (panel (d)). Black curves in panels (a)-(c) denote the curtain-ambient interface. Vertical dashed lines in panel (d) denote the forcing frequency values: $f = 0.76$ (black); $f = 5.34$ (red); $f = 11.43$ (blue). Here, $We = 2.5$ and $A_u = 0.1$.

the range $We \in [1.25, 10]$. Note that the Weber number variation is achieved by varying the surface tension coefficient σ. As a valuable result of the present analysis, Fig. 3(b)-(c) show that both the resonance frequency f_{max} and the corresponding maximum amplitude $A_{h,max}$ exhibit an increasing trend with the Weber number, both following the scaling law $\propto We^{\frac{1}{3}}$. As a consequence, the average wavelength in resonance conditions scales as $\bar{\lambda}_{max} \propto We^{-\frac{1}{3}}$. Theoretical insights on these scaling laws are given in [22].

4 VOF simulations in 2D resonance conditions

The forcing frequency f effect on the two-dimensional curtain flow field obtained with VOF simulations for Weber number $We = 2.5$ and forcing amplitude $A_u = 0.1$ is reported in Fig. 4. In particular, the streamwise velocity perturbation $u'(x, y)$ contour is shown in panels (a)-(c) for $f = 0.76$, 5.34 and 11.43, respectively, which are the same values as previously considered in Section 3. The three forcing frequencies are also represented by the vertical dashed lines in panel (d), which reports the Fast Fourier Transform (FFT) of the thickness distribution temporal

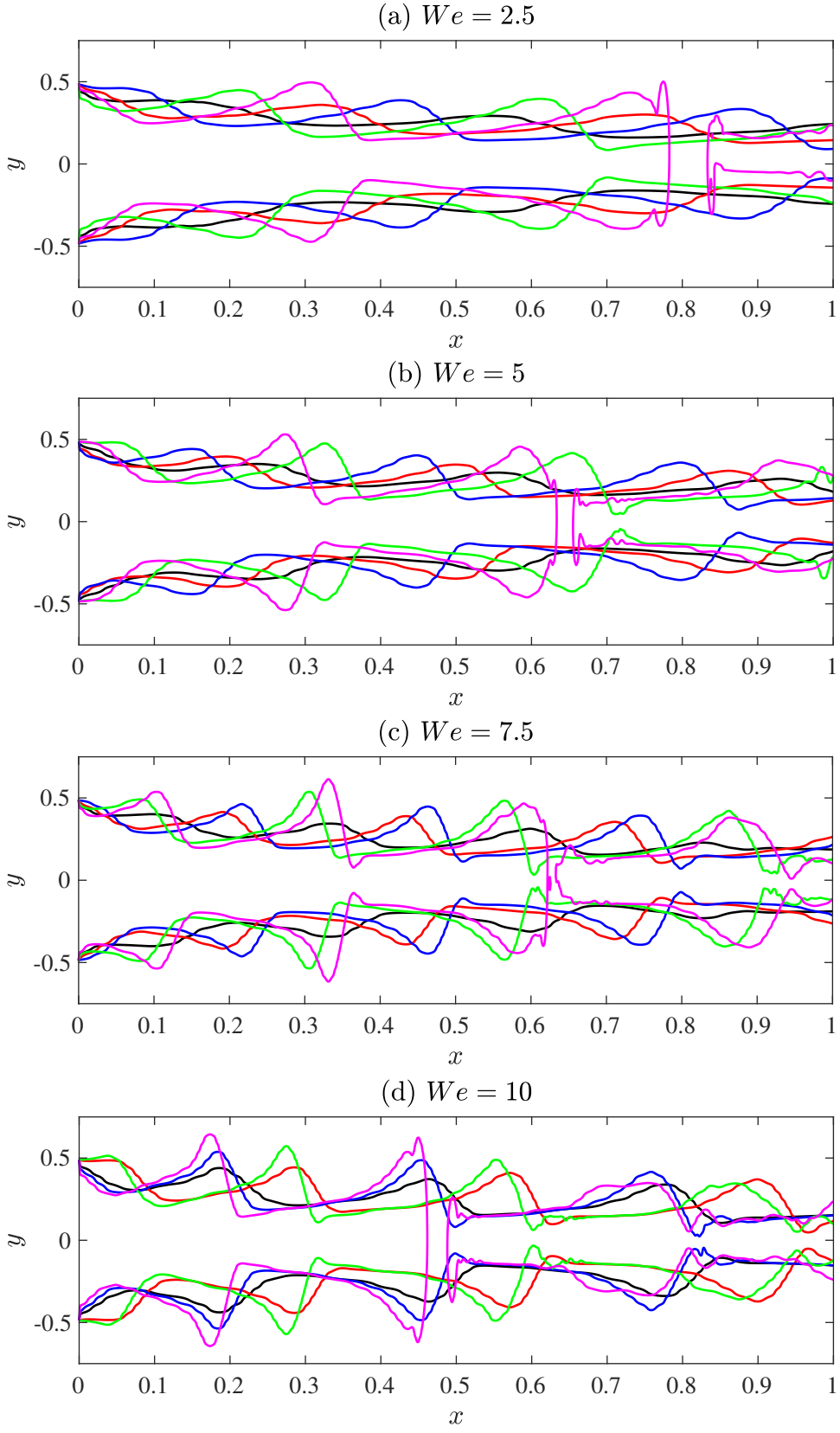

Figure 5: Curtain shape in resonance conditions for different values of the Weber number We by increasing the forcing amplitude A_u: 0.1 (black); 0.15 (red); 0.2 (blue); 0.25 (green); 0.3 (magenta).

signal $h'(t)$ at the streamwise station $x = 0.5$. Note that each curve in panel (d) is normalized with respect to the overall maximum.

The two-dimensional volume-of-fluid simulations confirm the one-dimensional linear analysis predictions: the curtain flow exhibits a resonance behaviour at $f = 5.34$ (Fig. 4(d)), for which the varicose oscillations of the curtain reach the maximum amplification. It is also interesting to observe that the varicose displacement of the two curtain-ambient interfaces induces analogous perturbations within the gaseous phase, as can be appreciated by looking at the symmetric (with respect to the axis $y = 0$) velocity contours distributions in Fig. 4(a)-(c). Note that a curtain-ambient interaction effect via velocity perturbations has also been found by [17] for a curtain subjected to a normal-to-flow (i.e. sinuous) velocity forcing.

The curtain dynamics in resonance conditions is further investigated in Fig. 5, which shows snapshots of the two-dimensional curtain shapes obtained for $f = f_{max}$ by varying the inlet forcing amplitude A_u, at the same Weber number values considered in Section 3. In particular, starting from the value $A_u = 0.1$ so far considered (black curves), the forcing amplitude is increased, and four more cases are investigated: $A_u = 0.15$ (red curves), 0.20 (blue curves), 0.25 (green curves) and 0.30 (magenta curves). The main result arising from the analysis of Fig. 5 is that, in resonance conditions, the curtain breaks up due to the reduction of its thickness induced by the varicose deformation. This thinning-induced numerical breakup results in the formation of an unsteady curtain fragmentation (see for example the magenta curve in Fig. 5(a) for $x \approx 0.8$), which is convected downstream along the curtain by the underlying gravitational base flow and expelled at the domain outlet (not shown in Fig. 5). It is worth pointing out that, once a "thin enough" sheet is created by means of the thinning physical mechanism, one may reasonably assume that the curtain will break due to short-range forces. On the other hand, we recall explicitly that such forces (or other non-equilibrium effects) are of course not included in the Navier-Stokes model here employed.

Interestingly, for each Weber number value considered, the reduction of curtain thickness induced by the varicose deformation (which leads to numerical breakup) occurs at a specific value of the forcing amplitude, i.e. $A_u = 0.30$, not depending on We. On the other hand, it can be seen that the streamwise station where this thinning occurs moves upstream by increasing the Weber number (e.g. it goes from $x \approx 0.8$ for $We = 2.5$, panel (a), to $x \approx 0.5$ for $We = 10$, panel (d)), i.e. it shifts downstream by considering progressively higher values of the surface tension coefficient, thus "spatially delaying" the breakup. In this respect, surface tension is found to play a stabilizing role on the varicose oscillations of the gravitational curtain. Note that a stabilizing effect of surface tension on the convective instability of unconfined planar liquid jets was also found by [23] by means of spatio-temporal stability analysis.

5 Conclusions

The varicose dynamics of a forced gravitational liquid sheet (curtain) issuing into a quiescent gaseous ambient has been numerically studied. The investigation has been performed in super-critical regime, namely for Weber number $We > 1$. Two methodologies have been employed: a simplified one-dimensional linear model, and two-dimensional volume-of-fluid (VOF) simulations. Employing harmonic forcing perturbations of the streamwise velocity applied at the inlet section, the varicose dynamics of the curtain has been excited and characterized by varying the forcing frequency f and amplitude A_u of the perturbations, for different values of We.

As a first significant result, the one-dimensional linear analysis has shown that the curtain oscillations amplitude reaches a maximum for a certain forcing frequency $f = f_{max}$. In other terms, it has been found that the flow manifests a resonance behaviour, with the natural oscillation frequency f_{max} and corresponding amplitude $A_{h,max}$ both scaling as $We^{\frac{1}{3}}$, while the average wavelength $\bar{\lambda}_{max}$ scales as $We^{-\frac{1}{3}}$. The two-dimensional VOF simulations have confirmed the one-dimensional model predictions of the flow natural frequency, as well as of the wavelength in resonance conditions.

It has been also found that the curtain breaks up numerically by increasing the forcing amplitude A_u, exhibiting a nonlinear saturated shape in incipient breakup conditions. The rupture is determined by a reduction of the curtain thickness induced by the varicose deformation, and it occurs at a specific value of the forcing amplitude, which does not depend on the Weber number. The streamwise station where the curtain thinning occurs moves upstream by increasing We, i.e. it shifts downstream by increasing the surface tension coefficient, thus "spatially delaying" the numerical breakup. In this respect, the surface tension is found to play a stabilizing role on the varicose oscillations of the curtain.

References

[1] S. P. Lin. Stability of a viscous liquid curtain. *Journal of Fluid Mechanics*, 104:111–118, 1981.

[2] Lord Rayleigh. *Theory of Sound*. Macmillan and Co., 1896.

[3] G.I. Taylor. The dynamics of thin sheets of fluid. III. disintegration of fluid sheets. *Proc. R. Soc. London Ser. A*, 253:313, 1959.

[4] A. Della Pia, A. Colanera, M. Chiatto, and L. de Luca. Energy insights into the unsteady dynamics of a viscous gravitational liquid sheet. *Physics of Fluids*, 33:092118, 2021.

[5] A. Colanera, A. Della Pia, and M. Chiatto. Data-driven global stability of vertical planar liquid jets by DMD on random perturbations. *Physics of Fluids*, 34:122101, 2022.

[6] A. Della Pia, A. Colanera, and M. Chiatto. Surface tension-induced instability in spatially developing subcritical liquid curtains. *Physics of Fluids*, 34:042122, 2022.

[7] L. de Luca and M. Costa. Instability of a spatially developing liquid sheet. *Journal of Fluid Mechanics*, 331:127–144, 1997.

[8] N. S. Barlow, B. T. Helenbrook, and S. P. Lin. Transience to instability in a liquid sheet. *Journal of Fluid Mechanics*, 666:358–390, 2011.

[9] S. J. Weinstein and K. J. Ruschak. Coating flows. *Annual Review of Fluid Mechanics*, 36:29–53, 2004.

[10] D. S. Finnicum, S. J. Weinstein, and K. J. Rushak. The effect of applied pressure on the shape of a two-dimensional liquid curtain falling under the influence of gravity. *Journal of Fluid Mechanics*, 255:647–665, 1993.

[11] S. J. Weinstein, A. Clarke, A.G. Moon, and E.A. Simister. Time-dependent equations governing the shape of a two-dimensional liquid curtain, part 1: Theory. *Physics of Fluids*, 9(12):3625–3636, 1997.

[12] F. De Rosa. Dinamiche instazionarie ed instabilità lineare globale di getti liquidi. In *PhD thesis, Università di Napoli Federico II, http://www.fedoa.unina.it/9459*, 2013.

[13] R. Scardovelli and S. Zaleski. Direct numerical simulation of free-surface and interfacial flow. *Annual Review of Fluid Mechanics*, 31(1):567–603, 1999.

[14] S. Popinet. Gerris: a tree-based adaptive solver for the incompressible Euler equations in complex geometries. *Journal of Computational Physics*, 190(2):572–600, 2003.

[15] S. Schmidt and K. Oberleithner. Instability of forced planar liquid jets: mean field analysis and non linear simulation. *Journal of Fluid Mechanics*, 883:1–38, 2020.

[16] S. Schmidt, O. Tammisola, L. Lesshafft, and K. Oberleithner. Global stability and nonlinear dynamics of wake flows with a two-fluid interface. *Journal of Fluid Mechanics*, 915:A96, 2021.

[17] A. Della Pia, M. Chiatto, and L. de Luca. Receptivity to forcing disturbances in subcritical liquid sheet flows. *Physics of Fluids*, 33:032113, 2021.

[18] J. A. van Hooft, S. Popinet, C. C. van Heerwaarden, S. J. A. van der Linden, S. R. de Roode, and B. J. H. van de Wiel. Towards adaptive grids for atmospheric boundary-layer simulations. *Boundary-Layer Meteorology*, 167(3):421–443, 2018.

[19] G. G. Agbaglah. Breakup of thin liquid sheets through hole-hole and hole-rim merging. *Journal of Fluid Mechanics*, 911:A23, 2021.

[20] M. M. Francois, S. J. Cummins, E. D. Dendy, D. B. Kothe, J. M. Sicilian, and M. W. Williams. A balanced-force algorithm for continuous and sharp interfacial surface tension models within a volume tracking framework. *Journal of Computational Physics*, 213(1):141–173, 2006.

[21] S. Popinet. An accurate adaptive solver for surface-tension-driven interfacial flows. *Journal of Computational Physics*, 228(16):5838–5866, 2009.

[22] A. Della Pia, M. Chiatto, and L. de Luca. Varicose dynamics of liquid curtain: linear analysis and volume-of-fluid simulations. *Physical Review Fluids*, 9(084003), 2024.

[23] M. R. Turner, J. J. Healey, S. S. Sazhin, and R. Piazzesi. Stability analysis and breakup length calculations for steady planar liquid jets. *Journal of Fluid Mechanics*, (668):384–411, 2011.